RSC Advances

This is an *Accepted Manuscript*, which has been through the Royal Society of Chemistry peer review process and has been accepted for publication.

Accepted Manuscripts are published online shortly after acceptance, before technical editing, formatting and proof reading. Using this free service, authors can make their results available to the community, in citable form, before we publish the edited article. This *Accepted Manuscript* will be replaced by the edited, formatted and paginated article as soon as this is available.

You can find more information about *Accepted Manuscripts* in the Information for Authors.

Please note that technical editing may introduce minor changes to the text and/or graphics, which may alter content. The journal's standard Terms & Conditions and the Ethical guidelines still apply. In no event shall the Royal Society of Chemistry be held responsible for any errors or omissions in this *Accepted Manuscript* or any consequences arising from the use of any information it contains.

ROYAL SOCIETY OF CHEMISTRY

www.rsc.org/advances

Journal Name

RSCPublishing

COMMUNICATION

Self-assembled monolayers of enantiomerically functionalized periodic mesoporous organosilicas and the effect of surface chirality on cell adhesion behaviour

Cite this: DOI: 10.1039/x0xx00000x

Received 00th January 2012,
Accepted 00th January 2012

DOI: 10.1039/x0xx00000x

www.rsc.org/

N. S. Kehr,*[a] H.-J. Galla,[b] K. Riehemann[a] and H. Fuchs[a]

In biotechnology, self-assembled monolayers (SAMs) of functionalized nanoparticles are of high interest as two dimentional (2D) surfaces to study cell-surface interactions. In this contribution, enantioselective functionalization of fluorescence dye loaded periodic mesoporous organosilicas (PMOs) with *D*(*L*)-mannose (MAN) and the preparation of the respective SAMs are described and the stereoselective interactions of these monolayers with different cell types are demonstrated. Cells do not only recognize the type of the surface functionality but also differentiate the surface chirality, which is much more pronounced in the presence of serum. Moreover, SAMs of PMO surfaces are used for the selective separation of malignant HeLa or C-6-Glioma cells from healthy endothelial cells. Finally PMOs are used as nanocontainers to deliver fluorescence dye molecules, as proof-of-principle for drug molecules, to the adhered cells on the SAM of PMOs.

Self-assembled monolayers (SAMs) of nanomaterials with specific chemical and physical properties have been widely used as two-dimensional (2D) artificial surfaces in biomedical research.[1] These hard materials are differ from the traditional soft polymer based biomaterials[2] due to their chemical composition, nanostructured character, large surface area, mechanical properties, porous nature, and their novel physical properties e.g. electronic, magnetic and optical properties that are usually not seen in single molecules or bulk materials. In addition, due to the advances in functionalization chemistry, the specific functionalization of their surfaces with bioactive ligands is an important tool to mimic extracellular matrix (ECM) and to control the interactions between cells and surfaces.[3,4] Recently, surface functionalization with chiral molecules has been used as effective parameter to control cell behaviours on material surfaces.[4d,4f,5,6,7] Although, the importance of chirality in biology, the interaction between chiral surfaces and biological systems have not been studied extensively. Recently we[4d,4f] and other groups[5,6,7] used surfaces which were enantiomerically functionalized with bioactive molecules (aminoacids or peptides) to investigate the chiral surface/biosystem interactions. In a pioneer work Sun *et al*. controlled the adhesion and morphology behavior of cells on enantiomerically functionalized gold or polymer brush film surfaces.[5a-d] Additionally, they showed that single-stranded DNA and protein have different adsorption behavior on enantiomophous surfaces.[7a-d] We described the functionalization of alginate hydrogels with enantiomers of bioactive aminoacids and the use of those alginate hydrogels as new 3D scaffolds for cell adhesion studies.[4f] We observed that the cells recognize and show different adhesion properties in the respective 3D hydrogel scaffolds. These results show clearly that chirality has fundamental and substantial effects on interactions between cells or biological systems and artificial surfaces. But these reports are limited to the use of enantiomers of bioactive molecules and substrate surfaces. Up to date only the enantiomers of aminoacids or peptides as bioactive molecules on flat material surfaces or polymer based systems as substrate surfaces have been used. The first example of the utilization of SAMs of enantiomorphous porous nanoobjects (zeolites L) as chiral substate surfaces to study the cell-chiral nanostructured surface interaction was reported by us.[4d] We showed the stereocontrolled interaction of different cell types on the respective SAMs of enantioselective functionalized zeolites L.[4d] The use of porous nanoobjects compared to flat surfaces allows us to take advantage of the pores of the particles which can host fluorescent dyes or biomolecules that can be used for imaging or drug delivery from 2D surfaces. Nevertheless, in order to learn more about chiral surface/biological system interactions, it is essential to examine different kinds of chiral systems, various cells and substrate surfaces.

In this contribution to go beyond the current state of the art of cell/chiral surface interaction, we present to the best of our knowledge for the first time, the combination of enantiomers of carbohydrate [*D(L)*-mannose (MAN)] as chiral molecules with SAMs of periodic mesoporous organosilicas (PMOs) as nanostructured surfaces. We report about the enantioselective functionalization of PMOs with enantiomers of *D*(*L*)-MAN, the

RSC Advances Accepted Manuscript

preparation of the respective SAMs of enantiomorphous PMOs, and the stereoselective interaction of these monolayers with different cell types. We show that cells have different adhesion behaviors depending on the used enantiomer for the enantiomerically functionalized PMO monolayers. Subsequently, SAMs of PMOs are used for the separation of primary cells and cancerous cells. Additionally, fluorescence dye loaded PMOs are applied as nanocontainers to stain adhered cells on SAMs of PMOs by release of fluorescence dye molecules as a prove of principle for drug delivery. The both enantiomers *D*- and *L*-mannose (MAN) were used as chiral end groups due to the importance of carbohydrates for biological systems,[8-10] PMO[11,12] was used as porous nanometer-scaled particle and as nanocontainer due to its unique properties e.g. high ordered mesopores which can be functionalized or loaded specifically with guest molecules for imaging, drug release or mass transport,[4e,13] high specific surface area, and easy surface functionalization.[11a,12a,4e,14]

D(*L*)-MAN was modified with a suitable linker according to procedures described in the literature[15] (for details see the SI, Fig. S1). Spherical amino functionalized PMOs (PMO-NH_2) were synthesized by co-condensation of 3-aminopropyltriethoxysilane (APTES) and 1,2-bis(trimethoxysilyl)ethane (BTME) in the presence of cetyltrimethylammonium bromide (CTAB)[16] (Fig. 1A). Then PMO-NH_2 was loaded with *N*,*N*'-bis(2,6-dimethylphenyl)perylene-3,4,9,10-tetracarboxylic diimide (DXP) fluorescent dye molecules (Fig. 1B) to get ^{DXP}PMO-NH_2. Subsequently, ^{DXP}PMO-NH_2 was functionalized with the *D*-MAN or *L*-MAN in the presence of EDC [1-ethyl-3-(3-dimethylamino-propyl)carbodiimide] and NHS (*N*-hydroxy-succinimide) to finally obtain ^{DXP}PMO-*D*-MAN and ^{DXP}PMO-*L*-MAN (Fig. 1C).

The SEM image of ^{DXP}PMO-NH_2 was composed of highly uniform and spherical shaped particles of approximately 250 nm in diameter (Fig. 1D). The particle size distribution of ^{DXP}PMO-NH_2 was confirmed by DLS (Fig. S2).

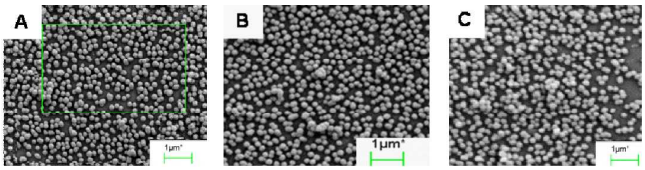

Fig. 2. SEM image of **A**.^{DXP}PMO-NH_2 (particles per µm²: 67) , **B.** ^{DXP}PMO-*D*-MAN (particles per µm²: 62), **C.** ^{DXP}PMO-*L*-MAN (particles per µm²: 66).

The IR bands of the ν(CO) and ν(CN) vibrations of the amide bonds of the ^{DXP}PMO-*D*-MAN and ^{DXP}PMO-*L*-MAN which are characteristic for amide I and amide II absorptions were observed at about 1642 cm^{-1} and 1586 cm^{-1} (Fig. S3B-C). In contrast ^{DXP}PMO-NH_2 shows no corresponding IR bands (Fig. S3A). In addition, OH and CH stretching vibrations occur in the 3100-3500 cm^{-1} and 2850-2950 cm^{-1} region respectively. As well the significant change of the zeta potential at pH 7.2 in phosphate buffered saline (PBS) buffer from 12.9 mV (^{DXP}PMO-NH_2) to -30.7 mV (^{DXP}PMO-*D*-MAN), -29.9 mV (^{DXP}PMO-*L*-MAN) indicates the successful functionalization of ^{DXP}PMO-NH_2 with *D*(*L*)-MAN. Using TGA we estimated the amount of loaded DXP dye in ^{DXP}PMO-*D*(*L*)-MAN to ca. 4 % w/w and the amount of functional groups (*D*- or *L*-MAN) to ca. 11 % w/w (Table S1 and Fig. S4). The number of both *D*- or *L*-MAN per surface area of PMOs was estimated at ca. 0.4 molecules per nm^2. A complete surface coverage should be 3.1 molecules per nm^2. The calculation was done according to the procedure described by Koberstein et. al.[17]

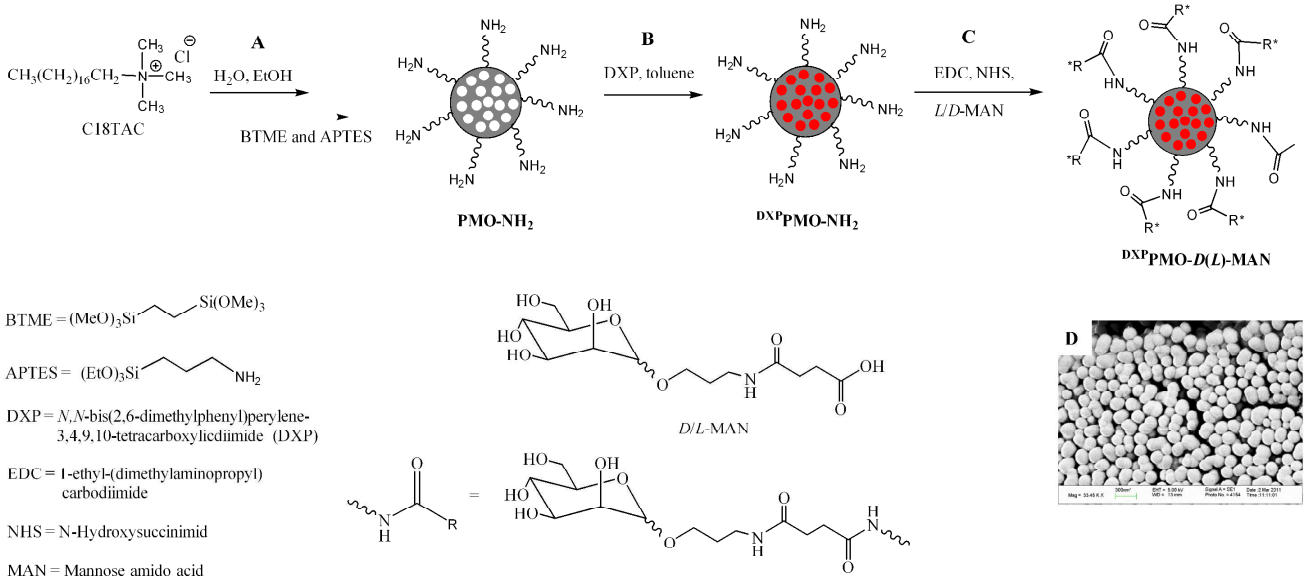

Fig. 1. Synthesis of **A**. PMO-NH_2, **B**. DXP loading of PMO-NH_2 to get ^{DXP}PMO-NH_2, **C**. functionalization of ^{DXP}PMO-NH_2 with *D*(*L*)-MAN to get ^{DXP}PMO-*D*(*L*)-MAN.

Attenuated total reflection infrared (ATR-IR) spectroscopy, zeta-potential measurements, scanning electron microscopy (SEM), thermogravimetric analyses (TGA) and dynamic light scattering (DLS) were used to characterize the ^{DXP}PMO-*D*-MAN and ^{DXP}PMO-*L*-MAN.

Then, SAMs of ^{DXP}PMO-*D*-MAN and ^{DXP}PMO-*L*-MAN, respectively, were prepared on glass slides which were pre-functionalized chemically with 3-chloropropyltrimethoxysilane. ^{DXP}PMO-*D*-MAN and ^{DXP}PMO-*L*-MAN were immobilized covalently on the functionalized glass slides according to sonication

RSC Advances Accepted Manuscript

This journal is © The Royal Society of Chemistry 2012

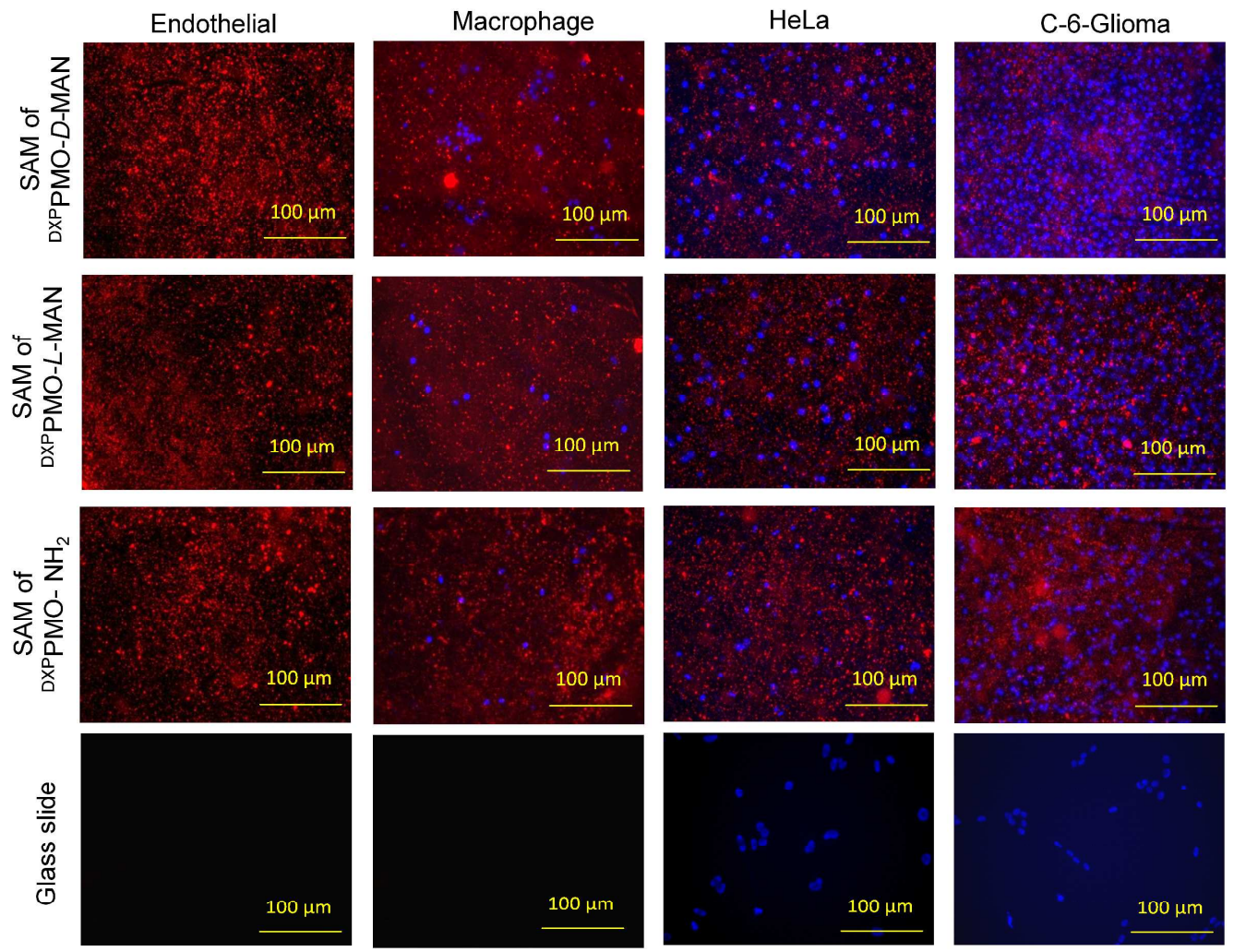

Fig. 3. Fluorescence microscope images of adhered endothelial, macrophage, HeLa, and C-6-Glioma cells (blue spots: DAPI stained cells) after 24 h incubation time (37 °C) on non-functionalized glass slide, SAMs of ^{DXP}PMO-NH_2, ^{DXP}PMO-*D*-MAN, and ^{DXP}PMO-*L*-MAN (red spots: DXP loaded PMO).

process described in the literature for other functionalized PMOs or zeolites (for details see the SI).[3e,4a,b] The SEM images of the obtained monolayers are depicted in the Fig. 2 (The particle distributions are homogeneous and the obtained particle density per μm^2 of ca. 65 are comparable to each other).

Subsequently, cell adhesion experiments on both SAMs of ^{DXP}PMO-*D*-MAN and ^{DXP}PMO-*L*-MAN were carried out (Fig.3 and Fig. 4). As control experiments the same cells were seeded on SAMs of ^{DXP}PMO-NH_2 and on a non-functionalized glass slide. Different cell types were used such as HeLa cells (derived from cervical cancer) and C-6 Glioma cells (rat astrocyte glioma cells) as cancerous cells or primary porcine brain capillary endothelial cells (PBCEC), and primary human macrophages (immune cells derived from peripheral blood) as healthy cells. Approximately the same amount of cells was separately seeded on two sets of SAMs of ^{DXP}PMO-*D*-MAN, SAMs of ^{DXP}PMO-*L*-MAN, SAMs of ^{DXP}PMO-NH_2, and non-functionalized glass slides. After 24 hours incubation the cell experiments were stopped. The adhered cells on the monolayers and on the glass slide of the first sets were washed, fixed and stained with 4',6-diamidino-2-phenylindole dihydrochloride

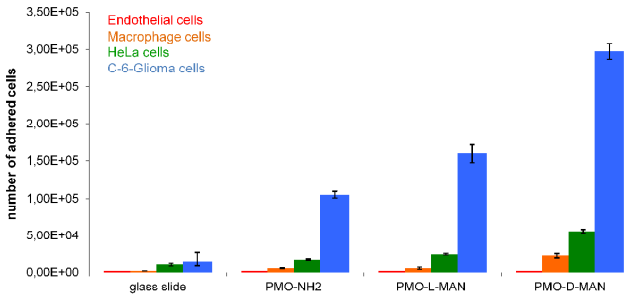

Fig. 4. Quantitative number of adhered endothelial, macrophage, HeLa and C-6-Glioma cells after 24 h incubation time (37°C) on glass slide, SAM of ^{DXP}PMO-NH_2, ^{DXP}PMO-*L*-MAN and ^{DXP}PMO-*D*-MAN (N= 3; *** data show significant differences; ANOVA-test: p≤ 0,001).

RSC Advances Accepted Manuscript

(DAPI) and the respective SAMs were analysed by fluorescence microscope (Fig. 3). The adhered cells of the second sets were washed, treated with trypsin and immediately counted using an automatic cell counter to obtain a quantitative number of adhered cells of the respective surfaces (Fig.4 and Table S2).

Our results showed that HeLa, C-6-Glioma and macrophage cells had higher affinity to SAMs of PMOs compared to non-functionalized glass slide. The reasons might be the differences of the hydrophobic character and/or nanostructured nature of the substrate surfaces as demonstrated by other groups.[18] SAMs of PMOs provide larger surface areas than glass slides. This results in a biomolecule functionalized monolayers, SAMs of ^{DXP}PMO-*D*-MAN and SAMs of ^{DXP}PMO-*L*-MAN. No cell clusters were visible at these fluorescence microscope images. But it seems that at the surfaces of the SAMs of ^{DXP}PMO-NH_2 small cell aggregates are visible (Fig. 3). On the contrary to the adhesion behavior of the used cancerous cell lines and healthy macrophage cells, other healthy endothelial cells did not adhere on respective monolayer surfaces at all. Eventhough we cannot explain without doubt the behaviour of healthy endothelial cells at this stage of our study. The reason might be the topography of the surfaces caused by the nanometer-scaled PMO particles.

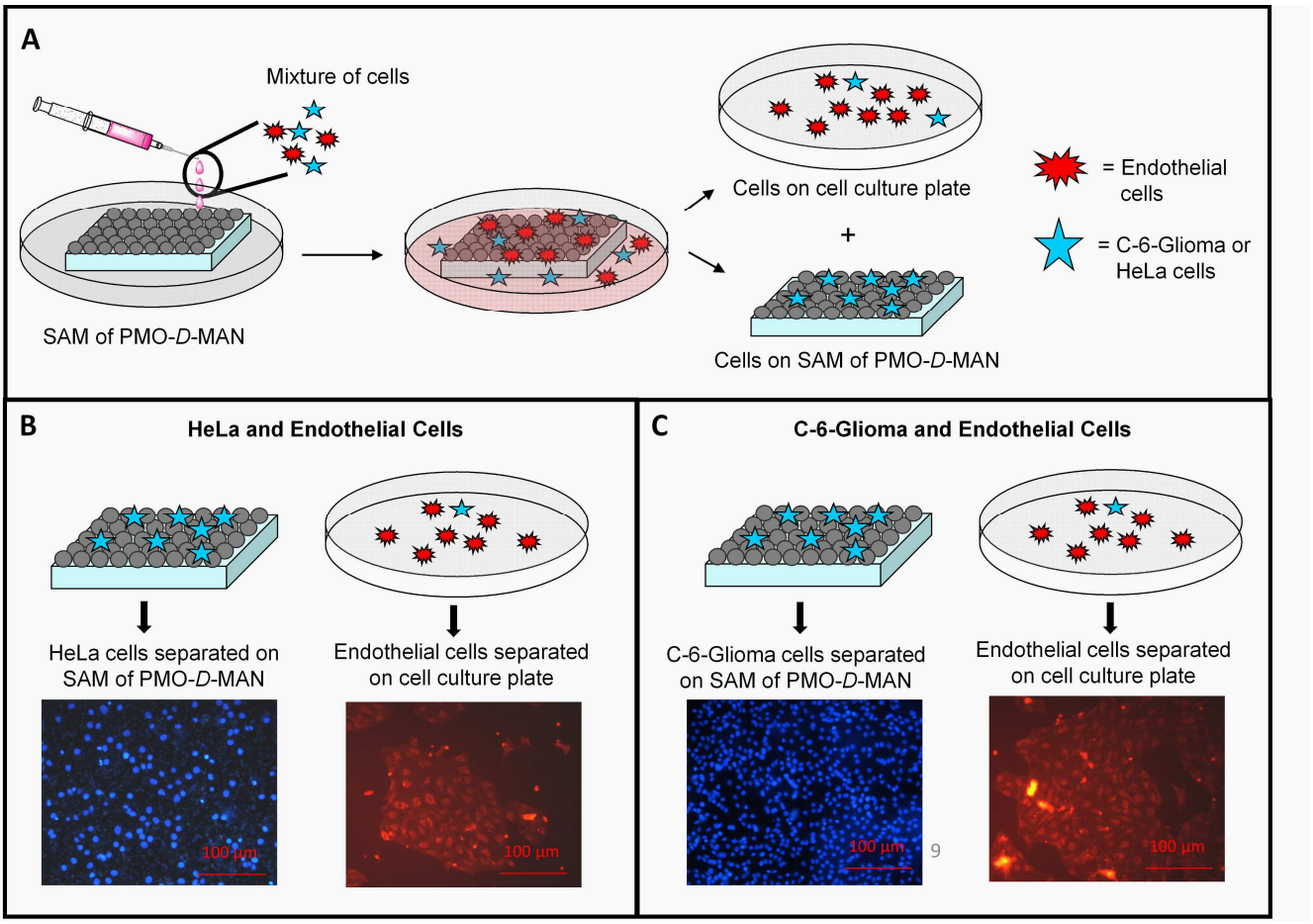

Fig. 5. (**A**) Schematic presentation of cell-cell separation. (**B**) HeLa or (**C**) C-6-Glioma and endothelial cells separation on SAM of PMO-*D*-MAN and cell culture plate (BP: 360-370 nm, BP: 530-550 nm, blue: DAPI stained HeLa or C-6-Glioma cell nucleus, red: Phalloidine Alexa Fluor® 546 stained endothelial cell membrane and actin filament).

higher number of contact points between cells and surfaces, and so a better cell adhesion on SAMs of PMOs. Moreover, the number of Hela and C-6-Glioma cells or macrophage on SAMs of ^{DXP}PMO-*D*-MAN was ca. 2 or 4 times higher than on SAMs of ^{DXP}PMO-*L*-MAN respectively. Similarly, number of Hela and C-6-glioma was ca. 3, macrophage cells was ca. 4 times higher on SAMs of ^{DXP}PMO-*D*-MAN than on the non-biomolecule modified SAMs of ^{DXP}PMO-NH_2 (Fig. 4 and Table S2). Statistical analysis shows that the quantitative number of adhered cells in different functional group is significant (N= 3; ***; ANOVA-test: $p \leq 0{,}001$). Simultaneously, it was possible to visualize the position of the cells on the SAMs of PMOs due to the fluorescent dye (DXP) inside of the bifunctionalized PMOs (Fig. 3). There is a nearly homogenous distribution of Hela, C-6-Glioma, and macrophage cells on both

We used this difference in cell adhesion behavior to separate HeLa or C-6-Glioma cancer cells from healthy endothelial cells. SAMs of PMO-*D*-MAN on glass were used as representative example. First we stained HeLa or C-6-Glioma cells with Hoechst dye molecules and endothelial cells with Phalloidin Alexa Fluor® 546. Then the respective 1:1 mixture of the stained HeLa / endothelial cells or C-6-Glioma / endothelial cells was added to the PMO-*D*-MAN monolayer in a cell culture plate (Fig. 5A). After 24 h incubation period the cell culture plate and the SAM of PMO-*D*-MAN were separated. The adhered cells on both surfaces were washed with PBS and fixed with 4% paraformaldehyde (PFA). Finally the both surfaces were analyzed by fluorescence microscopy. The fluorescence images (Fig. 5B and C) clearly showed that HeLa or C-6-Glioma cells were perfectly separated from endothelial cells

RSC Advances Accepted Manuscript

This journal is © The Royal Society of Chemistry 2012

by using PMO-*D*-MAN monolayer surfaces. Only blue fluorescent HeLa or C-6-Glioma cancer cells and no red fluorescent endothelial cells were observed on the PMO-*D*-MAN monolayers. Correspondingly, only red stained endothelial cells were detected on the respective cell culture plate.

MAN monolayer caused by the released of Hoechst 33342 dye from the pore of the PMO nanocontainers.

In order to prove that PMO particles were not uptaken by the cells themselves from the glass slide surface, and so the loaded Hoechst 33342 dye molecules were released intercellularly, we

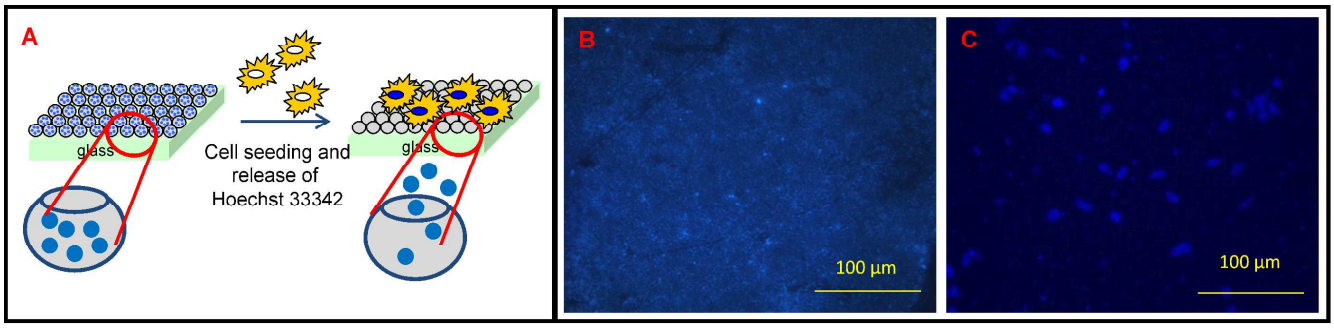

Fig. 6. (**A**) Schematic presentation of HeLa cell adhesion on SAM of ^{Hoechst}PMO-*D*-MAN and Hoechst 33342 release from the pores of ^{Hoechst}PMO-*D*-MAN. (**B**) Fluorescence microscopy image of SAMs of ^{Hoechst}PMO-*D*-MAN (BP: 360-370 nm, blue: Hoechst 33342 loaded PMOs). (**C**) Fluorescence microscopy image of HeLa cells on SAMs of ^{Hoechst}PMO-*D*-MAN (BP: 360-370 nm, blue: Hoechst 33342 stained cell nucleus).

We also carried out cell experiments in serum free cell culture media to describe the effects of protein adsorption on the cell adhesion behavior on SAMs of ^{DXP}PMO-*D*-MAN, SAMs of ^{DXP}PMO-*L*-MAN, SAMs of ^{DXP}PMO-NH_2 and on non-functionalized glass slide. Generally in all cases the numbers of adhered cells are lower in serum free media as in serum containing media. The quantity of adhered cell was higher on SAMs of PMOs compared to the non-functionalized glass slide. As well the number of adhered cells on the MAN functionalized surfaces was higher than the amount of cells on the non-biomolecule functionalized monolayer, and no adhesion of healthy endothelial and macrophage cells was observed (Table S2 and S3). But in contrast to the cell experiments carried out in the presence of serum, we observed approximatively the same affinity of HeLa and C-6-Glioma cells to SAM of ^{DXP}PMO-*D*-MAN and SAM of ^{DXP}PMO-*L*-MAN in serum free media (Table S3). These results showed that there should be a significant effect of protein adsorption not only on the cell affinity to the respective functionalized monolayer but also on the differentiation of the surface chirality of the used SAM of PMOs by the cells. We assume that suitable proteins of the serum interacts with the functional groups [*D*-(*L*)-MAN] at the surface of PMOs generating a stereochemical effect (e.g. diastereotopic effect) on the surface which is probably responsible for the observed cell adhesion behavior. Recent studies in this field suggest that non-covalent interactions between the chiral amino acids and the proteins could influence the adsorption behavior of proteins on chiral surfaces and so the differentiated cell adhesion behaviour on the respective chiral materials.[7d,c]

Finally, we used PMO-*D*-MAN particles as nanocontainers on 2D surfaces as representative example (Fig. 6). First PMOs were loaded with Hoechst 33342 (^{Hoechst}PMO-NH_2) followed by the functionalization of ^{Hoechst}PMO with *D*-MAN (^{Hoechst}PMO-*D*-MAN). Subsequently, SAM of ^{Hoechst}PMO-*D*-MAN was prepared and cell adhesion experiment with HeLa cells was performed (Fig. 6A, for detail see the SI). After the incubation period (24 h at 37 °C) SAM of ^{Hoechst}PMO-*D*-MAN was washed with PBS and the adhered HeLa cells were fixed with 4% PFA solution. The fluorescence microscopy image before adding HeLa cells shows the SAM of the Hoechst 33342 loaded PMOs on glass (Fig. 6B). Fig. 6C is the fluorescence microscopy image after the cell adhesion experiment and shows the blue stained Hela cell nuclei on the ^{Hoechst}PMO-*D*-

performed the following cell experiment on SAM of ^{DXP}PMO-*D*-MAN. HeLa cells were first grown on SAM of ^{DXP}PMO-*D*-MAN. After 24 hours incubation time the adhered HeLa cells on the ^{DXP}PMO-*D*-MAN monolayer were removed from the surface by trypsinization. Then one half of the cells were stained with DAPI and Phallodine Alexa Fluor® 488 in PBS and controlled by fluorescence microscopy (Fig 7C). The other half was seeded on non-functionalized glass substrate and incubated for 24 h. Subsequently, the adhered HeLa cells on glass substrate were washed with PBS, fixed with PFA, stained with DAPI and Phalloidin Alexa Fluor® 488 and analysed by fluorescence microscopy (Fig. 7D). The fluorescence microscopy images of SAM of ^{DXP}PMO-*D*-MAN before HeLa cell adhesion (Fig. 7A) and after the removal of the adhered HeLa cells (Fig. 7B) were examined as well. The respective fluorescence microscopy images of SAM of

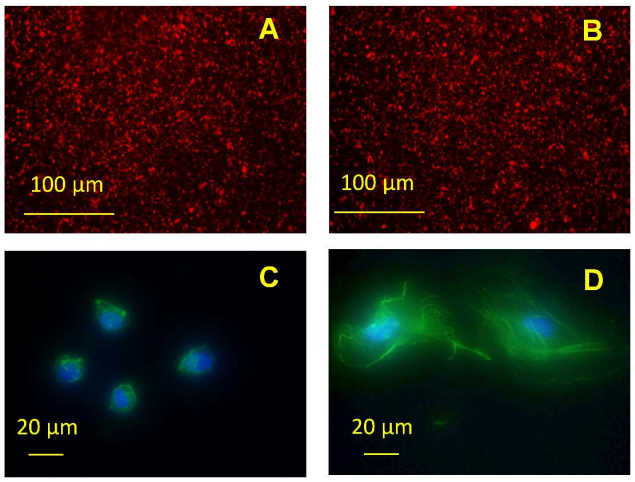

Fig.7. Fluorescence microscopy image of **A**. SAM of ^{DXP}PMO-*D*-MAN before HeLa cell adhesion, **B**. SAM of ^{DXP}PMO-*D*-MAN after the removal of adhered HeLa cells (BP: 530-550 nm, red: DXP loaded PMOs). Fluorescence microscopy merge image of **C.** HeLa cells in PBS, **D**. adhered HeLa cells on thenon-functionalized glass surface (BP: 360-370 nm, BP: 470-490 nm, BP: 530-550 nm, blue: DAPI stained HeLa cell nucleus, green: Phalloidin Alexa Fluor® 488 stained cell cytoskeleton and actin filament).

RSC Advances Accepted Manuscript

^{DXP}PMO-*D*-MAN (Figure 7A and 7B) show that red emitting dye (DXP) loaded PMO-*D*-MAN particles are still fixed on the glass surface. Moreover, fluorescence microscopy merge images of HeLa cells either in PBS solution (Fig. 7C) or adhered on the glass surface (Fig. 7D) didn't show any internalized red emitting DXP loaded particles [merge images were obtained at excitation range of 360-370 nm, 470-490 nm, and 530-550 nm to detect DAPI stained cell nucleus (blue), Phalloidin Alexa Fluor® 488 stained cell cytoskeleton and actin filament (green) and DXP loaded PMOs (red) respectively]. These results clearly show that PMO particles were not detached from the surface and penetrated into cells and so the release of Hoechst 33342 dye molecules from the pores of the respective PMO of the monolayer should be diffusion mediated.

Conclusions

In conclusion, we showed the successful enantioselective functionalization of fluorescence dye loaded PMOs with *D*- and *L*-MAN, respectively, and the preparation of the respective SAMs. We demonstrated that cell did not only recognize the type of the surface functionality but also differentiated the surface chirality, which was much more pronounced in the presence of serum. On the contrary to the cancerous HeLa, cancerous C-6-Glioma cells and healthy macrophage cells, health primary endothelial cells did not adhere on the respective monolayer surfaces at all. We used this different cell adhesion behavior to separate malignant HeLa or C-6-Glioma cell lines from healthy endothelial cells. Finally we used PMOs as nanocontainer to deliver fluorescence dye molecules, as proof-of-principle for drug molecules, to the adhered cells on the SAM of PMO-*D*-MAN. These results open new perspectives for the construction of suitable enantiomorphous SAM of nanomaterials (as ECM models) to understand cell/surface interactions more in detail. Furthermore not only the control of cellular behaviour (e.g cell/cell separation, cell adhesion, cell growth, cell differentiation etc.), but also the realization of new biocompatible surfaces for e.g. tissue engineering is envisaged. On the long term these results should allow us to design new 2D or 3D biomaterial surfaces as ECM models for biotechnological applications such as 2D and 3D cell culture systems, tissue engineering and drug delivery.

Acknowledgements

We thank DFG (TRR61) for funding and Judith Schmidt for technical assistance.

Notes and references

[a] Physikalishes Institut and CeNTech
Westfälische Wilhelms-Universität Münster
Heisenbergstraße 11, D-48149 Münster, Germany
E-mail: seda@uni-muenster.de
[b] Institut für Biochemie,
Westfälische Wilhelms-Universität Münster,
Wilhelm-Klemm-Str.2, D-48149 Münster, Germany

† Electronic Supplementary Information (ESI) available: [details of any supplementary information available should be included here]. See DOI: 10.1039/b000000x/

1 a) S. Zhang, *Nature Biotechnol*. 2003, **21,** 1171; b) N. J. Gleason, C. J. Nodes, E. M. Higham, N. Guckert, I. A. Aksay, J. E. Schwarzbauer, J. D. Carbeck, *Langmuir* 2003, **19**, 513; c) H. P. Zheng, M. C. Berg, M. F. Rubner, P. T. Hammond, *Langmuir* 2004, **20**, 7215; d) S. Zhang, X. Zhao, *J. Mater. Chem.* 2004, **14**, 2082; e) W. Kim, J. K. Ng, M. E. Kunitake, B, R, Conklin, P. D. Yang , *J. Am. Chem. Soc.* 2007, **129**, 7228; f) S. Wang, H. Wang, J. Jiao, K. J. Chen, G. E. Owens, K. Kamei, J. Sun, D. J. Sherman, C. P. Behrenbruch, H. Wu, H. R. Tseng, *Angew. Chem. Int. Ed.* 2009, **48**, 8970; g) C. G. Wilson, P. N. Sisco, F. A. Gadala-Maria, C. J. Murphy, E. C. Goldsmith, *Biomater.* 2009, **30**, 5639; h) H. J. Bai, M. L. Shao, H. L. Gou, J. J. Xu, H. J. Chen, *Langmuir* 2009, **25**, 10402; i) Y. Lai, C. Xie, Z. Zhang, W. Lu, J. Ding, *Biomaterials*, 2010, **31**, 4809.

2 a) A. Guiseppi-Elie, C, Dong, C. Z. Dinu, *J. Mater. Chem*., 2012, **22**, 19529; b) C. N. Kotanen, A. N. Wilson, C. Dong, C.-Z. Dinu, G. A. Justin, A. Guiseppi-Elie, *Biomaterials*, 2013, **34**, 6318.

3 a) R. Langer, J. P. Vacanti, *Science*, 1993, **260**, 920; b) A. Khademhosseini, J. P. Vacanti, R. Langer, *Sci. Am.* 2009, **300**, 64; c) X. Yao, R. Peng, J. Ding, *Adv. Mater*. 2013, **25**, 5257.

4 a) N. S. Kehr, K. Riehemann, J. El-Gindi, A. Schäfer, H. Fuchs, H. J. Galla, L. De Cola, *Adv. Funct. Mater.* 2010, **20**, 2248; b) N. S. Kehr, J. El-Gindi, H. J. Galla, L. De Cola, *Mic. Mes. Mater.* 2011, **144**, 9; c) O. Z. Fisher, B. L. Larson, D. Graupner, M. T. Nguyen-Kim, N. S. Kehr, L. De Cola, R. Langer, D. G. Anderson, *Adv. Mater.* 2012, **24**, 3032; d) J. El-Gindi, K. Benson, L. De Cola, H.-J. Galla, N. S. Kehr, *Angew. Chem. Int. Ed.* 2012, **51**, 3716; e) K. Benson, E. A. Prasetyanto, H-J. Galla, N. S. Kehr, *Soft Matter* 2012, **5**, 10845; f) K. Benson, H,-J, Galla, N. S. Kehr, *Macromol. Biosci*. 2014, **14**, 793; g) D. Böcking, O. Wiltschka, J. Niinimäki, H. Shokry, R. Brenner, M. Linden, C. Sahlgren, *Nanoscale*, 2014, **6**, 1490.

5 a) T. Sun, D. Han, K. Riehemann, L. Chi, H. Fuchs, *J. Am. Chem. Soc*. 2007, **129**, 1496; b) X. Wang, H. Gan, T. Sun, B. Su, H. Fuchs, D. Vestweber, S. Butz, *Soft Matter.* 2010, **6**, 3851; c) M. Zhang, G. Qing, T. Sun, *Chem. Soc. Rev*. 2012, **41**, 1972; d) X. Wang, H. Gan, M. Zhang, T. Sun, *Langmuir* 2012, **28**, 2791; e) W. Wei, C. Xu, N. Gao, J. Ren, X. Qu. *Chem. Sci.* 2014, DOI: 10.1039/C4SC01386G.

6 D. Hanein, B. Geiger, L. Addadi, *Science* 1994, **263**, 1413.

7 a) K. Tang, H. Gan, Y. Li, L. Chi, T. Sun, H. Fuchs, *J. Am. Chem. Soc.* 2008, **130**, 11284; b) H. Gan, K. Tang, T. Sun, M. Hirtz, Y. Li, L. Chi, S. Butz, H. Fuchs, *Angew. Chem. Int. Ed.* 2009, **48**, 5282; c) X. Wang, H. Gan,T. Sun, *Adv. Funct. Mater.* 2011, **21**, 3276; d) F, Zhou, L, Yuan, D. Li, H. Huang, T. Sun, H. Chen, *Colloids and Surfaces B: Biointerfaces,* 2012, **90**, 97; e) Z. Li, A. Köwitsch, G. Zhou, T. Groth, B. Fuhrmann, M. Niepel, E. Amado and J. Kressler, *Adv. Healthcare Mater.,* 2013, **2**, 1377; f) X. Yao, Y. Hu, B. Cao, R. Peng, J. Ding, *Biomaterials*, 2013, **34**, 9001.

8 a) G. Tosato, S. E. Pike, R. M. Blaese, *J. Exp. Med.* 1983, **158**, 1048; b) S. Park, M. R. Lee, I. Shin, *Chem. Commun*. 2008, **37**, 4389; c) C. Bhattacharya, Z. Yu, M. J. Rishel, S. M. Hecht, *Biochem.* 2014, **53**, 3264; d) M. M. Madathil, C. Bhattacharya, Z. Yu, R. Paul, M. J. Rishel, S. M. Hecht, *Biochem*. 2014, **53**, 6800; e) Z. Yu, R. M. Schmaltz, T. C. Bozeman, R. Paul, M. J. Rishel, K. S. Tsosie, S. M. Hecht, *J. Am. Chem. Soc*. 2013, **135**, 2883; f) B. R. Schroeder, M. I. Ghare, C. Bhattacharya, R. Paul, Z. Yu, P, A. Zaleski, T. C. Bozeman, M. J. Rishel, S. M. Hecht, *J. Am. Chem. Soc.* 2014, **136**, 1364.

9 a) T. Geijtenbeck, R. Torensama, S. van Vliet, G. van Duijnhoven, G. Adema, Y. van Kooyk, C. Figdor, *Cell* 2000, **100**, 575; b) D. M. Ratner, E. W. Adams, M. W. Disney, P. H. Seeberger, *ChemBioChem* 2004, **5**, 1375.

RSC Advances Accepted Manuscript

 This journal is © The Royal Society of Chemistry 2012

10 a) A. B. Boraston, D. N. Bolam, H. J. Gilbert, G. J. Davies, *Biochem. J.* 2004, **382**, 769; b) J. P. Kim, L. J. Olson, N. M. Dahms, *Curr. Opin. Struct. Biol*. 2009, **19**, 534; c) A. M. Wu, E. Lisowska, M. Duk, Z. Yang, *Glycoconjugate J*. 2009, **26**, 899.

11 a) S. Inagaki, S. Guan, Y. Fukushima, T. Ohsuna, O. Terasaki, *J. Am. Chem. Soc.* 1999, **121**, 9611; b) T. Asefa, M. J. MacLachlan, N. Coombs, G. A. Ozin, *Nature* 1999, **402**, 867; c) B. J. Melde, B. T. Holland, C. F. Blanford, A. Stein, *Chem. Mater.* 1999, **11**, 3302.

12 a) B. Hatton, K. Landskron, W. Whitnall, D. Perovic, G. A. Ozin, *Acc. Chem. Res*. 2005, **38**, 305; b) W. J. Hunks, G. A. Ozin, J. *Mater. Chem*. 2005, **15**, 3716; c) F. Hoffmann, M. Cornelius, J. Morell, M. Fröba, *Angew. Chem. Int. Ed*. 2006, **45**, 3216; *Angew. Chem.* 2006, **118**, 3290.

13 N. S. Kehr, E. A.Prasetyanto, K. Benson, B. Ergün, A. Galstyan, H.-J. Galla, *Angew. Chem. Int. Ed.,* 2013, **52**, 1156.

14 W. Guo, X. S. Zhao, *Microporous Mesoporous Mater*. 2005, **85**, 32.

15 K. El-Boubbou, C. Gruden, X. Huang, *J. Am. Chem. Soc.* 2007, **129**, 13392.

16 W. Guo, J. Wang, S. J. Lee, F. Dong, S. S. Park, and C. S. Ha, *Chem. Eur. J.* 2010, **16**, 8641.

17 S. Zhang, Y. Maidenberg, K. Luo, J. T. Koberstein, *Langmuir* 2014, **30**, 6071.

18 a) M. J. Dalby, M. O. Riehle, H. Johnstone, S. Affrossman, A. S. G. Curtis, *Biomater.* 2002, **23**, 2945; b) B. G. Cousins, P. J. Doherty, R. L. Williams, J. Fink, M. J. Garvey, *J. Mater. Sci. Mater. Med.* 2004, **15**, 355; c) S. Wang, H. Wang, J. Jiao, K. J. Chen, G. E. Owens, K. Kamei, J. Sun, D. J. Sherman, C. P. Behrenbruch, H. Wu, H. R. Tseng, *Angew. Chem. Int. Ed.* 2009, **48**, 8970; d) W. Luo, M. N. Yousaf, *Chem Commun.* 2009, 1237; e) M. Hulander, A. Lundgren, L. Faxälv, T. L. Lindahl, A. Palmquist, M. Berglin, H. Elwing, *Coll. Surf. B: Biointerfaces* 2013,**110***,* 261; f) Z. Lyu, H. Wang, Y. Wang, K. Ding, H. Liu, L. Yuan, X. Shi, M. Wang, Y. Wang, H. Chen, *Nanoscale*, 2014, **6**, 6959; g) Z. Novotna, A. Reznickova, O. Kvitek, N. S. Kasalkova, Z. Kolska, V. Svorcik, *Appl. Surf. Sci.* 2014, **307,** 217.

RSC Advances Accepted Manuscript